UCLA

UCLA Previously Published Works

Title
Wild-type Kras expands and exhausts hematopoietic stem cells

Permalink
https://escholarship.org/uc/item/5v29b1kq

Journal
JCI Insight, 3(11)

ISSN
2379-3708

Authors
Sasine, Joshua P
Himburg, Heather A
Termini, Christina M
et al.

Publication Date
2018-06-07

DOI
10.1172/jci.insight.98197

Peer reviewed

Wild-type Kras expands and exhausts hematopoietic stem cells

Joshua P. Sasine,[1,2,3,4] Heather A. Himburg,[1] Christina M. Termini,[1] Martina Roos,[1,3,4] Evelyn Tran,[1] Liman Zhao,[1] Jenny Kan,[1] Michelle Li,[1] Yurun Zhang,[1] Stéphanie C. de Barros,[5] Dinesh S. Rao,[1,3,4,5] Christopher M. Counter,[6] and John P. Chute[1,3,4]

[1]Division of Hematology/Oncology, Department of Medicine, [2]Molecular, Cellular and Integrative Physiology, [3]Jonsson Comprehensive Cancer Center, [4]Eli and Edythe Broad Center for Stem Cell Research, and [5]Department of Pathology and Laboratory Medicine, UCLA, Los Angeles, California, USA. [6]Department of Pharmacology and Cancer Biology, Duke University, Durham, North California, USA.

Oncogenic Kras expression specifically in hematopoietic stem cells (HSCs) induces a rapidly fatal myeloproliferative neoplasm in mice, suggesting that Kras signaling plays a dominant role in normal hematopoiesis. However, such a conclusion is based on expression of an oncogenic version of Kras. Hence, we sought to determine the effect of simply increasing the amount of endogenous wild-type Kras on HSC fate. To this end, we utilized a codon-optimized version of the murine *Kras* gene (*Kras^ex3op*) that we developed, in which silent mutations in exon 3 render the encoded mRNA more efficiently translated, leading to increased protein expression without disruption to the normal gene architecture. We found that Kras protein levels were significantly increased in bone marrow (BM) HSCs in *Kras^ex3op/ex3op* mice, demonstrating that the translation of Kras in HSCs is normally constrained by rare codons. *Kras^ex3op/ex3op* mice displayed expansion of BM HSCs, progenitor cells, and B lymphocytes, but no evidence of myeloproliferative disease or leukemia in mice followed for 12 months. BM HSCs from *Kras^ex3op/ex3op* mice demonstrated increased multilineage repopulating capacity in primary competitive transplantation assays, but secondary competitive transplants revealed exhaustion of long-term HSCs. Following total body irradiation, *Kras^ex3op/ex3op* mice displayed accelerated hematologic recovery and increased survival. Mechanistically, HSCs from *Kras^ex3op/ex3op* mice demonstrated increased proliferation at baseline, with a corresponding increase in Erk1/2 phosphorylation and cyclin-dependent kinase 4 and 6 (Cdk4/6) activation. Furthermore, both the enhanced colony-forming capacity and in vivo repopulating capacity of HSCs from *Kras^ex3op/ex3op* mice were dependent on Cdk4/6 activation. Finally, BM transplantation studies revealed that augmented Kras expression produced expansion of HSCs, progenitor cells, and B cells in a hematopoietic cell–autonomous manner, independent from effects on the BM microenvironment. This study provides fundamental demonstration of codon usage in a mammal having a biological consequence, which may speak to the importance of codon usage in mammalian biology.

Introduction

The mammalian RAS family is composed of 3 genes that encode 4 small GTPase proteins: HRAS, NRAS, KRAS4A, and KRAS4B in humans and Hras, Nras, Kras4a, and Kras4b in mice (1, 2). RAS proteins transmit signals from surface receptors to intracellular signaling proteins (1–4). RAS proteins share 79% amino acid sequence identity, with variability residing in the last 25 amino acids that encode sites of post-translational modifications (1, 5). The nucleotide sequences are more divergent, with *KRAS* preferentially encoded by A or T at wobble base pairs, whereas *HRAS* is encoded by G or C, and NRAS by a mixture of all 4 nucleotides (1, 6). Codons ending in A or T are rare in mammalian exomes and rare codons have been shown to impede the efficiency of translation elongation (1, 7). Consistent with this, the rare codons in *KRAS* have been shown to impede translation of the encoded mRNA, reducing protein expression (1, 6).

Current understanding of the role of RAS signaling in the hematopoietic system has been driven primarily by studies in which oncogenic mutant *Ras* transgenes were overexpressed in bone marrow (BM) hematopoietic stem cells (HSCs) and progenitor cells (8–18). Varied hematopoietic effects have been observed, depending on the mutant *Ras* transgene overexpressed and the mouse model itself.

MacKenzie et al. (8) showed that 60% of recipient mice injected with BM cells transduced with a retrovirus encoding oncogenic *Nras* developed a variety of myeloid malignancies after prolonged latency. Mx1-Cre-LoxP–driven induction of endogenous but oncogenic *Nras* in hematopoietic cells caused the development of indolent myeloproliferative disease in mice and potentiated the development of additional hematologic cancers (12). Enforced expression of a single allele of oncogenic *Nras* using the Mx1-Cre model also increased HSC proliferation and serial repopulating capacity, providing possible explanation for the clonal advantage conferred by oncogenic *Nras* expression (13). Furthermore, the dosage of Ras protein has been shown to correlate with the transformative effects of *Ras* oncogenes in the murine hematopoietic system (12, 14). Transplantation of primary murine hematopoietic cells transduced with a vector encoding oncogenic *Hras* produced lymphomas and lymphoid leukemias in mice (16). In contrast, inducible expression of an *Mx1-Cre*–driven oncogenic version of the endogenous *Kras* gene in BM hematopoietic cells caused a rapidly fatal myeloproliferative disease in mice (9). Subsequent studies showed that activating this mutant allele in BM ckit+lin− progenitor cells caused aberrant signaling downstream, as well as increased HSC competitive repopulating fitness and the ability to initiate T-lineage leukemias following transplantation (11). Recently, expression of oncogenic *Kras* in Flt-3+ multipotent progenitor cells caused a neonatal myeloid leukemia in mice with features that recapitulated human juvenile myelomonocytic leukemia (18). Importantly, pharmacologic inhibition of the downstream effectors of Ras, specifically MEK and PI3K, has been shown to abrogate oncogenic Kras–driven myeloproliferative disease in mice, suggesting that interruption of RAS-driven signaling could ameliorate disease progression in patients with hematologic malignancies and RAS mutations (15, 19).

The above findings suggest an important role for Kras in normal hematopoiesis. However, this has not been directly tested since oncogenic Ras proteins, often overexpressed, have been used to chronically drive high levels of Ras signaling. It is known that Kras is required for adult hematopoiesis (20), but these studies abolished the gene, and hence, the extent to which Kras signaling underlies normal hematopoiesis remains unclear (20). Interestingly, retrovirus-mediated overexpression of oncogenic HRAS in human cord blood lin− cells induced a high level of HRAS signaling, decreased proliferation, and enhanced monocyte differentiation (17). Fine-tuning the activation levels in these cells with a farnesyltransferase inhibitor produced a smaller increase in HRAS signaling and promoted a hematopoietic blast-like cell phenotype and self-renewal (17). Consistent with this observation, overexpression of a single allele of oncogenic *Nras* increased HSC repopulating capacity in mice (13). Furthermore, the BM niche–derived paracrine factor, pleiotrophin, promotes HSC regeneration in irradiated mice via upregulation of Ras/MEK/ERK signaling (21, 22). These results suggest that moderate amplification in Ras signaling could promote the expansion of HSCs and progenitor cells.

In order to directly test this hypothesis, we utilized a version of the *Kras* gene that generates higher levels of the wild-type Kras protein without altering the normal gene architecture. More specifically, we utilized the *Kras^{ex3op}* gene, which was created by introducing 33 silent mutations into exon 3 of the endogenous *Kras* gene to change 27 rare codons to their common counterparts to optimize translation, which produces a 2- to 4-fold increase in Kras protein compared with the unaltered allele (1). We show here that a mere 2-fold increase in the amount of Kras in the hematopoietic compartment led to an increase in HSC proliferation and short-term repopulating capacity as measured in primary competitive transplantation assays, while substantially improving hematopoietic regeneration and survival in mice following high-dose irradiation. However, these positive effects ultimately led to the exhaustion of long-term HSCs (LT-HSCs), as measured in competitive secondary transplantation assays. Taken together, these results reveal the nuanced physiologic function of wild-type Kras in regulating HSC fate and suggest that augmentation of Kras signaling has therapeutic potential for the immediate management of myelosuppression. Moreover, this study demonstrates that codon usage in a mammal has biological consequences, which speaks to the importance of codon usage in mammalian biology.

Results

Translation of Kras protein in BM HSCs is constrained by rare codons. We sought to determine the effect of increased Kras protein levels on HSC fate. To this end, we utilized the aforementioned murine *Kras^{ex3op}* allele, which produces higher levels of wild-type Kras protein without altering the protein sequence or architecture of the gene (1). Homozygous *Kras^{ex3op/ex3op}* mice displayed a 2-fold increase in Kras protein levels with no abnormal splice variants, overt developmental phenotypes, or changes in lifespan (6). In order to validate a
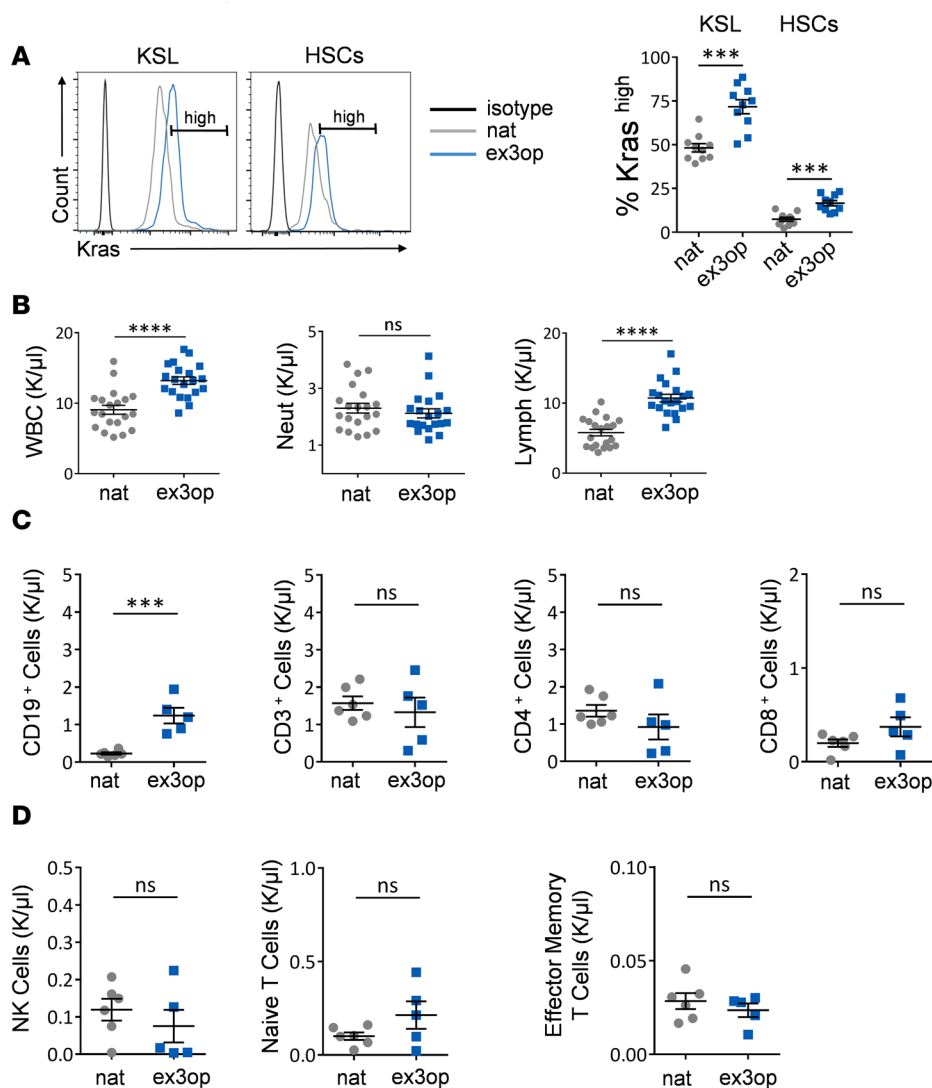
JCI insight

Figure 1. Kras translation is constrained by rare codons and increased Kras expands B lymphocytes. (**A**) At left, representative histograms of Kras protein levels in BM KSL cells and HSCs in 8- to 12-week-old *Kras^ex3op/ex3op* mice (*ex3op*) and *Kras^nat/nat* mice (*nat*). Isotype control is shown in black. Gate represents Kras^hi cells. At right, mean percentages of Kras^hi cells are shown within each mouse group (*n* = 9/group). ***P < 0.001. (**B**) Scatter plots show mean PB white blood cells (WBCs), neutrophils (Neut), and lymphocytes (Lymph) at baseline in 8- to 12-week-old *Kras^ex3op/ex3op* and *Kras^nat/nat* mice (*n* = 20/group). ****P < 0.0001. (**C** and **D**) Scatter plots show the numbers of PB CD19⁺ B cells, CD3⁺ T cells, CD4⁺ T cells, CD8⁺ T cells, NK cells, naive T cells, and effector memory T cells (*n* = 8/group). ***P < 0.001. Two-tailed Student's *t* test was used for each comparison. ns, not significant. Data are presented as mean ± SEM.

similar increase in the hematopoietic system, we measured Kras protein levels in BM ckit⁺sca1⁺lin⁻ (KSL) hematopoietic stem/progenitor cells (HSPCs) and CD150⁺CD48⁻KSL HSCs from *Kras^ex3op/ex3op* mice versus mice expressing native *Kras* (*Kras^nat/nat* mice; Figure 1A). *Kras^ex3op/ex3op* mice displayed significantly increased percentages of Kras^hi KSL cells and Kras^hi HSCs compared with control *Kras^nat/nat* mice, confirming that the replacement of rare codons with common codons in exon 3 of *Kras* does indeed increase Kras protein levels in the HSC and progenitor populations. Of note, the relative levels of Kras protein were increased in BM KSL progenitor cells compared with BM HSCs in both *Kras^ex3op/ex3op* mice and *Kras^nat/nat* mice, consistent with prior studies demonstrating that protein translation overall is higher in progenitor cells than in HSCs (23).

Kras^ex3op/ex3op mice display lymphocytosis and expansion of CD19⁺ B cells. Hematologic analysis of 8- to 12-week-old *Kras^ex3op/ex3op* mice and *Kras^nat/nat* mice revealed an increase in peripheral blood white blood cells (PB WBCs) and lymphocytes in *Kras^ex3op/ex3op* mice compared with control mice, whereas no differences in neutrophils, hemoglobin, or platelet counts were observed (Figure 1B and Supplemental Figure 1A; supplemental material available online with this article; https://doi.org/10.1172/jci.insight.98197DS1). Flow cytometric analysis of PB lymphocyte subsets demonstrated that the lymphocytosis was caused by an increase in CD19⁺ B cells (Figure 1C). We observed no differences in the numbers of PB CD3⁺, CD4⁺, or CD8⁺ T cells and no differences in PB natural killer (NK) cells, naive T cells, or memory T cells (Figure 1, C and D). Analysis of percentages of T cell subsets in the thymus of 8-week-old *Kras^ex3op/ex3op* mice and control mice also revealed no differences in T cell subsets or progenitors (Supplemental Figure 1, B–D). Finally, BM analysis revealed increased BM cell counts in *Kras^ex3op/ex3op* mice compared with *Kras^nat/nat* mice at baseline,
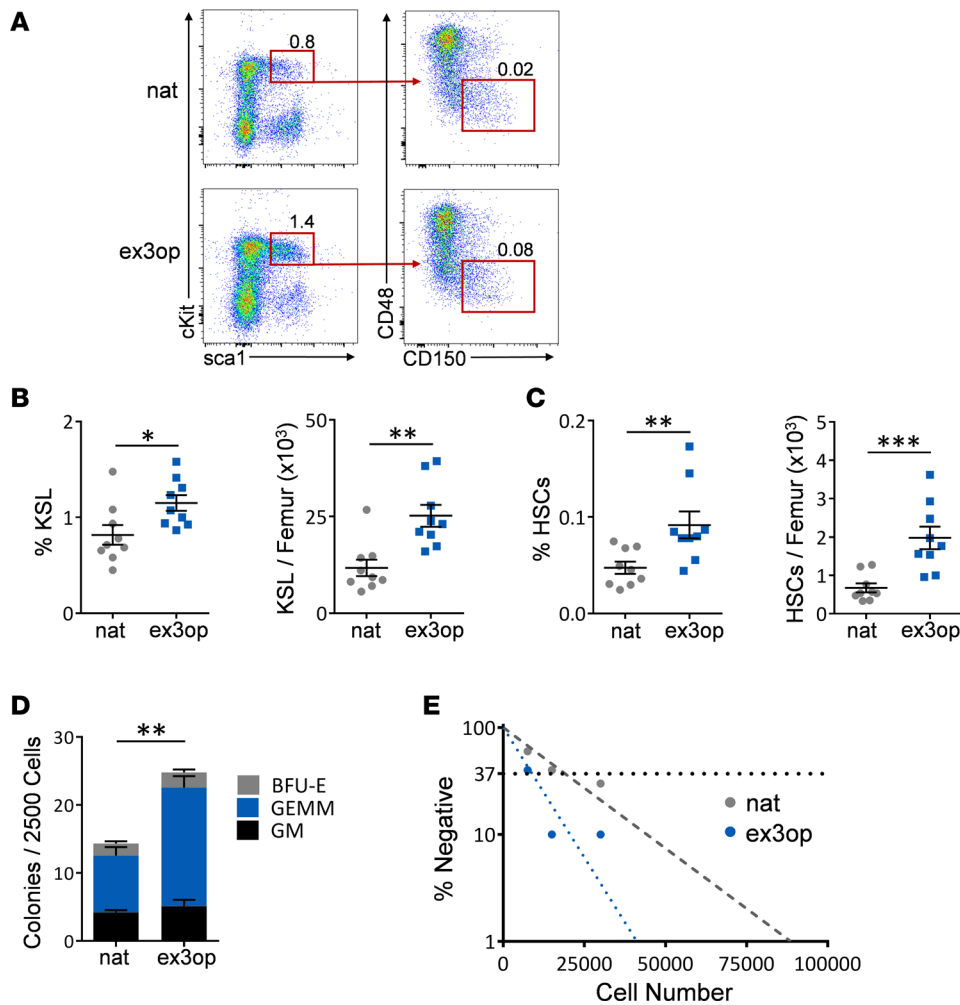
Figure 2. *Kras^ex3op/ex3op* mice display increased BM HSCs and progenitor cells. (**A**) Representative flow cytometric analysis of BM ckit⁺sca1⁺lin⁻ (KSL) cells and CD150⁺CD48⁻KSL HSCs in *ex3op* mice and *nat* mice at baseline. Numbers represent the percentages of KSL cells and CD150⁺CD48⁻KSL cells shown within the gates. (**B**) Mean percentages of BM KSL cells and numbers of KSL cells in *ex3op* mice and *nat* mice at baseline (*n* = 9/group). *P < 0.05, **P < 0.01. (**C**) Mean percentages of BM HSCs and numbers of HSCs in *ex3op* mice and *nat* mice (*n* = 9/group). **P < 0.01, ***P < 0.001. (**D**) Mean numbers of CFCs in *ex3op* mice and *nat* mice (*n* = 10/group). **P < 0.01. (**E**) Poisson statistical analysis of a limiting-dilution assay revealed BM LTC-IC frequencies of 1 in 8,940 in *ex3op* mice and 1 in 19,235 in *nat* mice at 8–12 weeks. The plot shows the percentage of negative colonies detected at 3 different BM cell doses. The horizontal line represents the cell dose at which 37% of the plates show no colonies (*n* = 6/group). *P* = 0.03. Two-tailed Student's *t* test performed throughout. Data are presented as mean ± SEM.

but no differences were observed in the percentages of BM common lymphoid progenitor cells (CLPs), myelo-erythroid progenitor cells (MEPs), or granulocyte monocyte progenitor cells (GMPs) (Supplemental Figure 1, E and G). A small increase in the percentage of BM common myeloid progenitor cells (CMPs) was observed in *Kras^ex3op/ex3op* mice (Supplemental Figure 1G). We observed no differences in spleen mass between *Kras^ex3op/ex3op* mice and *Kras^nat/nat* mice (Supplemental Figure 1F).

Kras^ex3op/ex3op mice display HSC expansion and exhaustion of long-term repopulating HSCs. *Kras^ex3op/ex3op* mice displayed increased percentages and numbers of BM KSL cells and phenotypic HSCs compared with *Kras^nat/nat* mice (Figure 2, A–C). *Kras^ex3op/ex3op* mice also contained increased numbers of BM colony-forming cells (CFCs) and long-term culture–initiating cells (LTC-ICs) compared with control mice (Figure 2, D and E). Taken together, these results suggested that increased Kras protein expanded both phenotypic HSCs and progenitor cells.

We next performed competitive repopulation assays to determine if *Kras^ex3op/ex3op* mice contained increased functional HSC content. For this purpose, *Kras^ex3op/ex3op* and *Kras^nat/nat* mice were backcrossed more than 10 generations into C57BL/6 mice (CD45.2⁺) and we utilized syngeneic recipient B6.SJL mice (CD45.1⁺) as recipients. Recipient mice transplanted competitively with 2 × 10⁵ BM cells (CD45.2⁺) from *Kras^ex3op/ex3op* mice, along with 2 × 10⁵ competitor (CD45.1⁺) BM cells, displayed significantly increased total donor CD45.2⁺ cell engraftment over time compared with mice transplanted with an equal dose of BM cells from *Kras^nat/nat* mice (Figure 3, A and B). Recipient mice transplanted with BM cells from *Kras^ex3op/ex3op* mice also displayed increased engraftment of donor cells within the myeloid, B cell, and T cell lineages through 20 weeks compared with recipient mice transplanted with BM cells from *Kras^nat/nat* mice (Figure 3, A–C, and Supplemental Figure 2A) (24–27).

In order to assess for LT-HSC content in *Kras^ex3op/ex3op* mice, we performed secondary competitive repopulation assays using 1 × 10⁶ BM cells collected from primary recipient mice at 20 weeks after transplant, along with 2 × 10⁵ competitor BM cells. Of note, as we have previously observed and has been demonstrated by
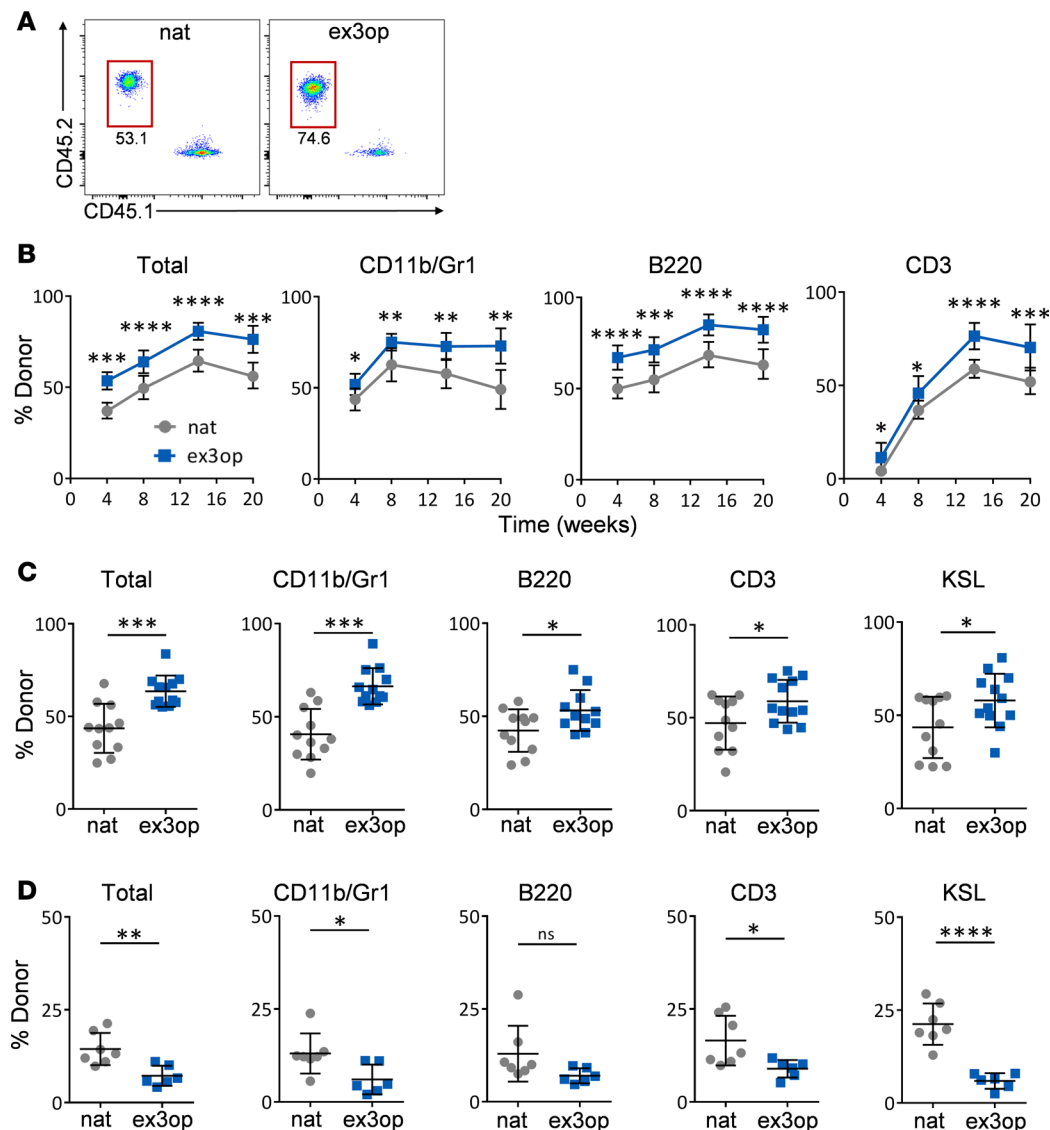
Figure 3. Increased wild-type Kras expands HSCs and exhausts long-term repopulating HSCs. (**A**) Representative flow cytometric analysis of donor CD45.2+ hematopoietic cell engraftment in the PB of recipient CD45.1+ mice at 20 weeks following transplantation of 2×10^5 BM cells from *ex3op* mice or *nat* mice, along with 2×10^5 competitor CD45.1+ BM cells. Numbers represent percentages in each gate. (**B**) Panels show the mean percentages (± SD) of total donor CD45.2+ cells and donor CD45.2+ cells within the CD11b+ myeloid population, B220+ B cells, and CD3+ T cells in the PB of CD45.1+ recipient mice over time following competitive transplantation of BM cells from *ex3op* mice (CD45.2+) or *nat* mice (CD45.2+) (n = 12/group). *P < 0.05, **P < 0.01, ***P < 0.001, ****P < 0.0001. (**C**) Mean percentages (± SD) of total donor CD45.2+ cells and donor CD45.2+ cells within the BM CD11b+ myeloid population, B220+ B cells, CD3+ T cells, and KSL population in CD45.1+ recipient mice at 20 weeks following competitive transplantation of BM cells from *ex3op* mice or *nat* mice (n = 12/group). *P < 0.05, ***P < 0.001. (**D**) Panels show the percentages of donor (DsRed+) total cell engraftment, as well as donor cell engraftment within CD11b+ myeloid cells, B220+ B cells, CD3+ T cells, and KSL cells in the BM of secondary recipient (Ds-Red negative) mice at 16 weeks following competitive transplantation of 1×10^6 BM cells collected from primary recipient mice. Primary recipient (Ds-Red negative) mice were transplanted with 2×10^5 BM cells from *Kras^{ex3op/ex3op}* (Ds-Red positive) mice or *Kras^{nat/nat}* (Ds-Red positive) mice, along with 2×10^5 competitor (DsRed-negative) BM cells (n = 7/group). *P < 0.05, **P < 0.01, ****P < 0.0001. Data are presented as mean ± SD. Two-tailed Student's *t* test was used for all analyses.

others (28, 29), overall donor cell engraftment decreased in competitively transplanted secondary mice in both groups compared with engraftment levels in primary recipient mice (Figure 3D). However, secondary recipient mice transplanted with BM cells from primary recipient mice in the *Kras^{ex3op/ex3op}* mice group demonstrated significantly decreased donor hematopoietic cell engraftment at 16 weeks after transplant compared with mice transplanted with control BM cells (Figure 3D). This exhaustion of hematopoietic repopulating capacity was most evident within CD11b+ myeloid cells, CD3+ T cells, and in the BM KSL population in secondary recipients (Figure 3D). These results suggest that a small increase in Kras protein levels caused the expansion of HSCs with short-term repopulating capacity, but yielded the exhaustion of LT-HSCs.
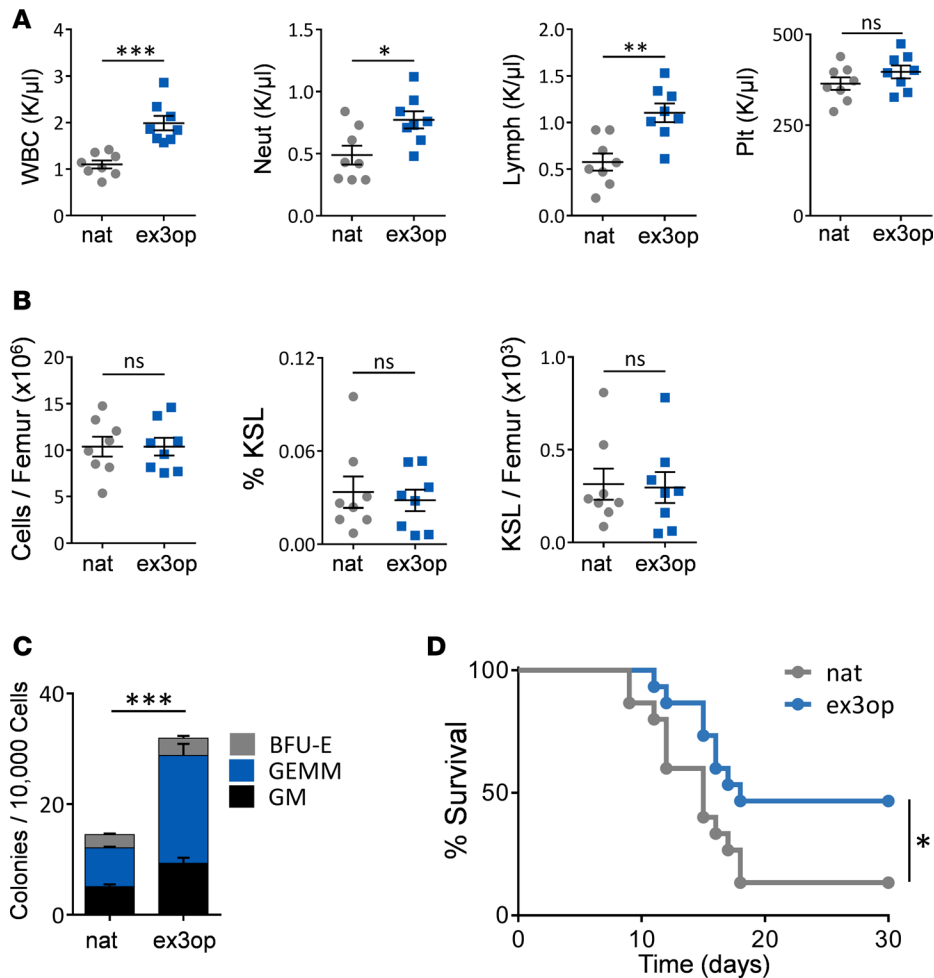
Figure 4. Increased wild-type Kras promotes hematopoietic regeneration following myelosuppression. (**A**) Mean PB WBCs, neutrophils, lymphocytes, and platelet (Plt) counts are shown in *ex3op* mice and *nat* mice at day +14 following 750 cGy TBI (*n* = 10/group). *P < 0.05, **P < 0.01, ***P < 0.001. ns, non-significant. (**B**) Mean BM cell counts, percentage of KSL cells, and numbers of KSL cells at day +14 following 750 cGy (*n* = 10/group). (**C**) Mean numbers of BM CFCs at day +14 (*n* = 10/group). ***P < 0.001. (**D**) The percentage survival of *ex3op* mice and *nat* mice is shown through day +30 following 750 cGy TBI (*n* = 12/group). *P = 0.03 by log-rank test for survival analysis. For all other analyses, 2-tailed Student's *t* tests were performed. Data are presented as mean ± SEM.

Kras$^{ex3op/ex3op}$ mice display augmented hematopoietic regeneration following myelosuppression. Since BM HSCs in *Kras$^{ex3op/ex3op}$* mice displayed increased colony-forming capacity and competitive repopulating capacity in primary recipient mice, we hypothesized that *Kras$^{ex3op/ex3op}$* mice would have augmented hematopoietic regenerative capacity following myelosuppression. We therefore irradiated *Kras$^{ex3op/ex3op}$* mice and *Kras$^{nat/nat}$* mice with 750 cGy total body irradiation (TBI), which causes severe myelosuppression, and evaluated hematopoietic recovery in both groups. At day +14, *Kras$^{ex3op/ex3op}$* mice displayed accelerated recovery of PB WBCs, neutrophils, and lymphocytes compared with control mice (Figure 4A). We observed no difference in BM cell counts or in percentages or numbers of BM KSL cells or ckit$^+$sca1$^-$lin$^-$ myeloid progenitors between *Kras$^{ex3op/ex3op}$* mice and *Kras$^{nat/nat}$* mice at day +14 following irradiation (Figure 4B and Supplemental Figure 2B). However, *Kras$^{ex3op/ex3op}$* mice contained significantly increased BM CFCs at day +14 compared with *Kras$^{nat/nat}$* mice (Figure 4C). The accelerated recovery of myelopoiesis and mature neutrophils in *Kras$^{ex3op/ex3op}$* mice was also associated with a significant improvement in survival following TBI. Eight of 17 *Kras$^{ex3op/ex3op}$* mice (46%) remained alive at day +30 following 750 cGy TBI, compared with 2 of 17 of the *Kras$^{nat/nat}$* mice (14%, P = 0.03, Figure 4D).

Kras$^{ex3op/ex3op}$ mice do not develop myeloproliferative disease or leukemia. Since mice expressing oncogenic versions of either Kras or Nras develop myeloproliferative disease or hematologic cancers over time, we sought to determine whether increasing levels wild-type Kras protein would similarly promote myeloid disease evolution (8, 9). *Kras$^{ex3op/ex3op}$* mice did not develop myeloproliferative disease or myelodysplasia and no splenomegaly was observed through 20 months of age (Supplemental Figure 3, A–D). We also did not observe gross changes in the BM microenvironment in *Kras$^{ex3op/ex3op}$* mice over time (data not shown). Detailed immunophenotypic analysis also suggested no myeloid or lymphoid skewing at 20 months of age (Supplemental Figure 3, B and D). Lastly, we detected no germline mutations in *Kras*, *Hras*, or *Nras* in *Kras$^{ex3op/ex3op}$* mice to account for the observed hematopoietic phenotype in young adult mice (data not shown).
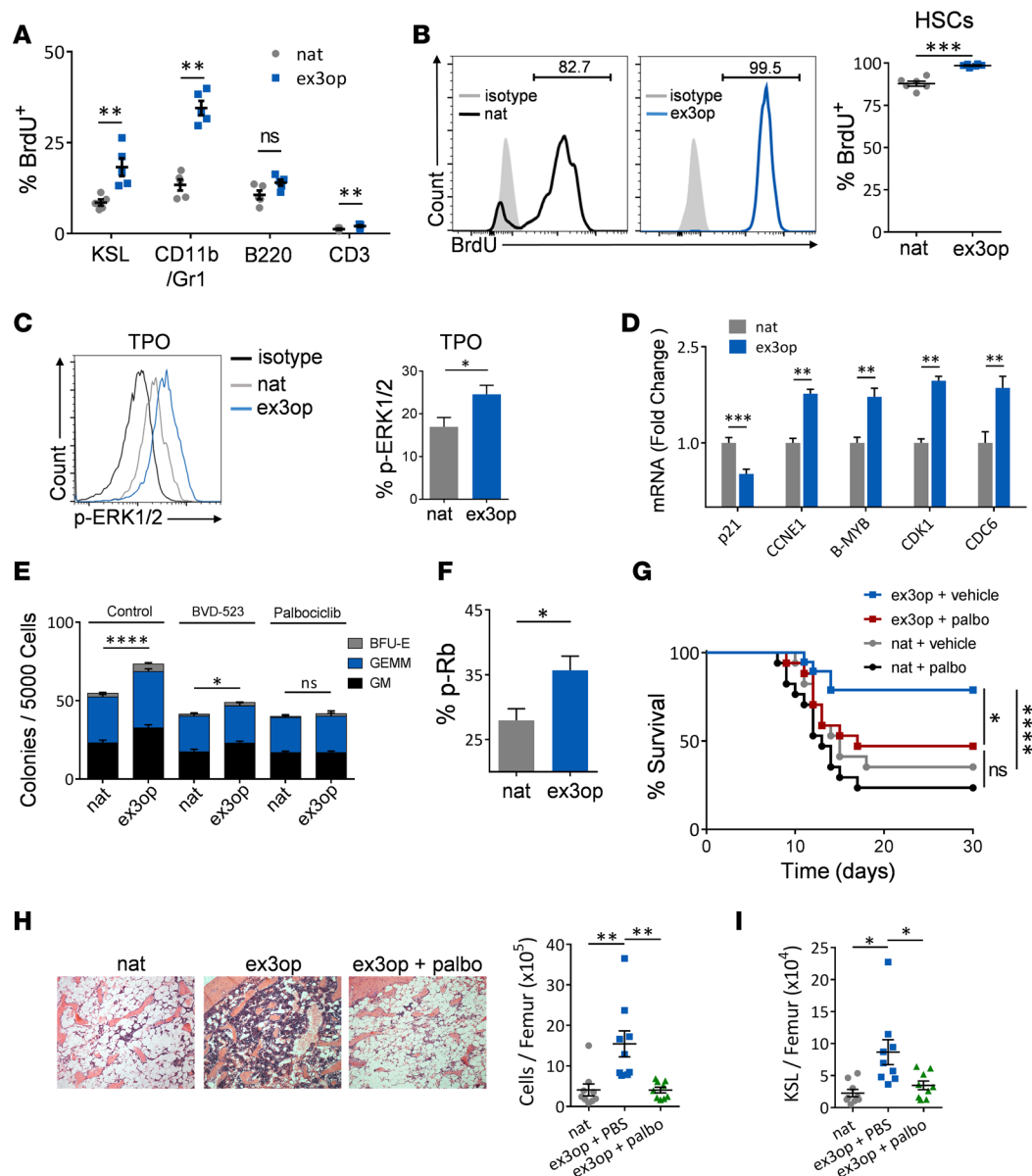
Figure 5. Wild-type Kras augments hematopoietic repopulating capacity in a Cdk4/6–dependent manner. (**A**) Increased percentage of BrdU-positive cells are shown within BM KSL cells, myeloid cells, B cells, and T cells in *ex3op* mice compared with *nat* mice at 24 hours after BrdU administration (*n* = 5/group). **P < 0.01. (**B**) At left, representative analysis of BrdU incorporation in BM CD150+CD48−KSL HSCs in *nat* mice and *ex3op* mice at day +25 following continuous BrdU administration in drinking water. At right, mean percentages of BrdU-positive HSCs are shown in each group (*n* = 6/group). ***P < 0.001. (**C**) At left, representative phospho-Erk1/2 (p-Erk1/2) expression in BM KSL cells from *ex3op* mice and *nat* mice in response to 20 ng/ml thrombopoietin (TPO) treatment for 5 minutes. At right, bar graphs show p-Erk1/2–positive KSL cells in each group (*n* = 5/group). *P < 0.05. (**D**) Relative mRNA levels of cell cycle regulatory genes in BM KSL cells from *ex3op* mice and *nat* mice at baseline (*n* = 8/group). **P < 0.01, ***P < 0.001. (**E**) Mean numbers of CFCs following 72-hour culture of BM KSL cells from *ex3op* mice or *nat* mice with media containing TPO, stem cell factor, and Flt-3 ligand (TSF), with or without the Erk1/2 inhibitor, BVD-523, or the Cdk4/6 inhibitor, palbociclib (palbo) (*n* = 6/group). *P < 0.05, ****P < 0.0001. (**F**) Mean percentages of phospho-Rb (p-Rb) in BM KSL cells in *ex3op* mice and *nat* mice at baseline (*n* = 4/group). *P < 0.05. (**G**) Adult C57BL/6 mice were irradiated with 850 cGy TBI, and then transplanted with 1 × 10^{5} BM cells from *ex3op* mice or *nat* mice and treated on days +5 and +6 with either 85 mg/kg palbo or saline. Percentage survival of each group of mice is shown (*n* = 17/group). Log-rank test was used for survival analysis. *P < 0.05, ****P < 0.0001. (**H**) At left, representative microscopic images of femurs stained with H&E (×10 magnification) at day +14 from irradiated mice transplanted with *ex3op* BM cells, *nat* BM cells, or *ex3op* BM cells + palbociclib treatment. At right, mean BM cell counts (± SEM) at day +14 are shown for each group (*n* = 9/group). **P < 0.01. (**I**) Scatter plot shows numbers of BM KSL cells at day +14 in irradiated recipient mice transplanted with *nat* BM cells, *ex3op* BM cells, and *ex3op* BM cells + palbo treatment (*n* = 9). *P < 0.05. Except as noted, P values were obtained using a 2-tailed Student's *t* test. Data are presented as mean ± SEM.
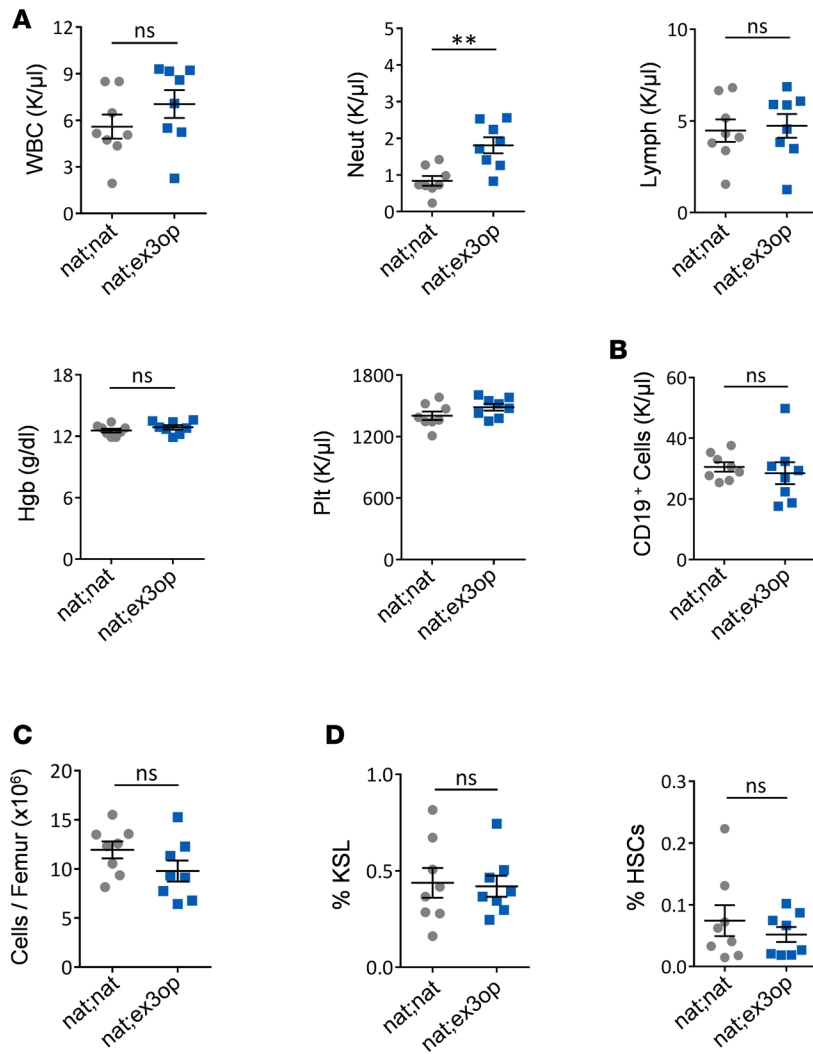
Figure 6. Kras regulates hematopoiesis in a hematopoietic cell–autonomous manner. (A) Scatter plots show no differences in PB WBCs, lymphocytes, hemoglobin (Hgb), or platelets (Plt) between 8-week-old *nat;ex3op* mice and *nat;nat* mice. Increased PB neutrophils are detected in *nat;ex3op* mice (*n* = 8/group). *******P* < 0.01. **(B)** Mean numbers of PB CD19+ B cells and **(C)** BM cell counts in each group (*n* = 8/group). **(D)** Percentages of BM KSL and HSCs from each group (*n* = 8/group). Data are presented as mean ± SEM. Two-tailed Student's *t* test was used for all analyses. ns, not significant.

HSCs in Kras^ex3op/ex3op^ mice demonstrate an increase in Cdk4/6–dependent repopulating capacity. Ras proteins transduce information from the cell surface that regulates numerous cellular mechanisms, including proliferation, differentiation, and survival (1, 6, 9, 17, 30–33). Since *Kras^ex3op/ex3op^* mice displayed expansion of phenotypic and functional HSCs and progenitor cells, we compared the baseline proliferation status and survival of HSCs in *Kras^ex3op/ex3op^* mice versus *Kras^nat/nat^* mice. Twenty-four hours following administration of BrdU, *Kras^ex3op/ex3op^* mice demonstrated significantly increased proliferation of BM KSL cells, ckit+sca1–lin– myeloid progenitors, CD11b/Gr1+ myeloid cells, and CD3+ T cells, but no difference in proliferation of CLPs or B220+ B cells compared with control mice (Figure 5A and Supplemental Figure 4, A and B). After continuous BrdU administration, we also observed substantially increased BrdU incorporation in BM HSCs at day +5 and day +25 in *Kras^ex3op/ex3op^* mice (Figure 5B and Supplemental Figure 4, C and D). Following 750 cGy TBI, BM KSL cells and ckit+sca1–lin– myeloid progenitors in *Kras^ex3op/ex3op^* mice also displayed increased BrdU incorporation compared with KSL cells and myeloid progenitors from irradiated, control mice (Supplemental Figure 4E). We observed no differences in annexin+7AAD+ cells or annexin+7AAD– cells within BM HSCs, BM KSL cells, or B cells between *Kras^ex3op/ex3op^* mice and *Kras^nat/nat^* mice at baseline, suggesting no effect of increased Kras protein levels on the survival of HSCs, progenitor cells, or B cells (Supplemental Figure 4, F and G). We also detected no difference in the homing capacity of BM cells from *Kras^ex3op/ex3op^* mice compared with *Kras^nat/nat^* mice as an explanation for the increased in vivo repopulating capacity (Supplemental Figure 4H).

Consistent with increased stimulation of the Ras pathway, BM KSL cells from *Kras^ex3op/ex3op^* mice displayed elevated phospho-Erk1/2 (p-Erk1/2) levels in response to thrombopoietin (TPO) alone or the combination of TPO/SCF/Flt-3 ligand compared with KSL cells from *Kras^nat/nat^* mice (Figure 5C and

Supplemental Figure 5A). We note here that no differences were observed in p-Akt, p-STAT5, or p-S6 levels in BM KSL cells from $Kras^{ex3op/ex3op}$ mice versus $Kras^{nat/nat}$ mice in response to TPO (Supplemental Figure 5B). We also found no alterations in the expression of $Cdkn2d$ and $Cdkn1b$, which encode the cell cycle inhibitors, p19 and p27, respectively, in BM KSL cells from $Kras^{ex3op/ex3op}$ mice, but expression of $Cdkn1a$, which encodes the cell cycle inhibitor, p21, was significantly decreased (Figure 5D and Supplemental Figure 5C) (34–36). Treatment of BM KSL cells from $Kras^{ex3op/ex3op}$ mice with the Erk1/2 inhibitor, BVD-523, abrogated the expansion of BM hematopoietic progenitor cells observed in $Kras^{ex3op/ex3op}$ mice, suggesting that the amplification of the hematopoietic compartment in $Kras^{ex3op/ex3op}$ mice was mediated through Erk1/2 (Figure 5E). We hypothesized further that Erk1/2–mediated suppression of p21 might be contributing to HSC proliferation in $Kras^{ex3op/ex3op}$ mice by relieving p21-mediated inhibition of cyclin-dependent kinases (Cdks) (28, 29). Indeed, BM KSL cells from $Kras^{ex3op/ex3op}$ mice displayed significantly increased levels of phosphorylated retinoblastoma tumor suppressor protein (p-Rb), consistent with inactivation of Rb by either Cdk4/cyclin D or Cdk2/cyclin E (Figure 5F) (37, 38). Further, we observed increased expression of E2F-regulated cell cycle regulatory genes, including Ccne1, B-myb, and Cdk1, in BM KSL cells in $Kras^{ex3op/ex3op}$ mice, in keeping with Rb inactivation (Figure 5D) (39–41). Importantly, treatment of BM KSL cells from $Kras^{ex3op/ex3op}$ mice with the Cdk4/6 inhibitor, palbociclib, suppressed the amplification of BM hematopoietic progenitors, suggesting that the increased HSC proliferative capacity was dependent on Erk1/2–mediated augmentation of Cdk4/6 activation (Figure 5E). In order to determine if the enhanced in vivo repopulating capacity of HSCs in $Kras^{ex3op/ex3op}$ mice was also dependent on Cdk4/6 activation, we performed BM transplantation of 1×10^5 BM cells from $Kras^{ex3op/ex3op}$ mice versus $Kras^{nat/nat}$ mice into syngeneic recipient mice and then treated recipient mice with or without palbociclib. Mice transplanted with a limiting dose of BM cells from $Kras^{ex3op/ex3op}$ mice displayed increased survival compared with recipients of the identical dose of BM cells from control $Kras^{nat/nat}$ mice (Figure 5G). However, treatment with palbociclib abrogated the augmented in vivo repopulating capacity of BM cells from $Kras^{ex3op/ex3op}$ mice, yielding significantly decreased survival (Figure 5G). At day +14, mice transplanted with BM cells from $Kras^{ex3op/ex3op}$ mice displayed accelerated recovery of BM cell counts and KSL stem/progenitor cells compared with mice transplanted with BM from $Kras^{nat/nat}$ mice, while treatment with palbociclib suppressed this augmented hematopoietic recovery in recipients of $Kras^{ex3op/ex3op}$ BM cells (Figure 5, H and I). These results suggested that the augmented regenerative capacity of hematopoietic stem/progenitor cells in $Kras^{ex3op/ex3op}$ mice was dependent on Cdk4/6 activation.

Kras regulates hematopoiesis in a cell-autonomous manner. In order to determine if the hematopoietic effects observed in $Kras^{ex3op/ex3op}$ mice were cell autonomous in nature, we transplanted wild-type ($Kras^{nat/nat}$) BM cells into irradiated $Kras^{ex3op/ex3op}$ mice to generate chimeric *nat;ex3op* mice. In order to control for the TBI and transplantation effects, we compared the hematopoietic phenotype of *nat;ex3op* mice with that of control mice transplanted with $Kras^{nat/nat}$ BM cells (*nat;nat* mice, controls). At 8 weeks after transplant, all mice in both groups demonstrated high donor chimerism (range 91%–98%) in the PB. Analysis of the PB of *nat;ex3op* mice revealed no increases in PB WBCs, lymphocytes, or B cells compared with control mice and no differences in BM cell counts, KSL cells, or HSCs between *nat;ex3op* mice and control mice (Figure 6, A–D). A small increase in PB neutrophils was noted in *nat;ex3op* mice compared with control mice. These results suggested that the amplification of HSCs, progenitor cells, and B cells observed in $Kras^{ex3op/ex3op}$ mice was caused by hematopoietic cell–autonomous effects of increased wild-type Kras, rather than indirect effects via the BM microenvironment.

Discussion

Activating an oncogenic version of the endogenous *Kras* gene in the hematopoietic system results in a fatal myeloproliferative disease characterized by hypersensitivity to growth factors and hyperproliferation (9), suggesting that Kras plays a critical role in normal hematopoiesis. In order to directly test this hypothesis, we took advantage of a novel approach to studying signaling biology, namely producing more protein through silent mutations that change codon usage without altering any other feature of the gene. Using this approach, we demonstrate that increasing wild-type Kras protein levels in BM HSCs of $Kras^{ex3op/ex3op}$ mice promotes the proliferation and expansion of HSCs capable of primary competitive repopulation and increased hematopoietic regeneration following irradiation, without any evidence of myeloproliferative disease or leukemia. Admittedly, while no mutations in *Ras* genes were detected, we cannot rule out that the higher levels of wild-type Kras did not promote the expansion of HSCs with other mutations, and it

remains to be determined whether such an increase could predispose other oncogenic mutations to be more leukemogenic. However, the highly penetrant phenotype and normal appearance of the BM suggests that the increased regenerative capacity of HSCs was a feature of elevated Kras protein expression. Interestingly, elevated Kras ultimately led to exhaustion of LT-HSCs in secondary transplantation assays, indicating that this proliferative effect has an upper limit. We contrast our observation with prior studies using *Mx1-Cre;Nras*[G12D/+] mice, which showed that expression of a single allele of the *Nras-G12D* oncogene in the hematopoietic compartment increased LT-HSC function as measured by serial transplantation assays (13). While we did not perform limiting-dilution assays to estimate HSC frequency in this study, our competitive secondary transplant assays suggested a loss of LT-HSCs in *Kras*[ex3op/ex3op] mice. The divergent effects of wild-type *Kras* expression and *Nras-G12D* expression on LT-HSC function may be related to fundamental differences in Kras and Nras cellular activities (42, 43), or sustained *Nras* oncogene expression versus wild-type *Kras* expression. In this regard, Ras dosage has been shown to promote unique effects on hematopoietic cells and the observed loss of LT-HSC repopulating capacity in *Kras*[ex3op/ex3op] mice may be a function of modest Ras dosage relative to Ras oncogene models (12, 14).

Kras[ex3op/ex3op] mice also displayed PB lymphocytosis, which was caused by increased CD19^{+} B cells in the absence of alterations in T cell populations. This observation contrasts with the described effects of oncogenic *Kras-G12D* expression in the hematopoietic compartment, which produced a rapidly fatal myeloproliferative disease in mice (9–11). However, conditional deletion of *Kras* in the hematopoietic compartment in mice was associated with decreased B cell numbers, in addition to increased neutrophil counts and splenomegaly (20). This result, coupled with our findings, suggest that wild-type Kras has a physiologic role in regulating B cell content.

We show that elevated levels of wild-type Kras augment the hematopoietic colony–forming capacity of HSCs, which is dependent on Erk1/2 activation. In the activated state, Erk1/2 translocates to the nucleus and regulates the activity of several transcription factors, including c-Jun, c-Myc, and c-Fos, which in turn induce or repress the expression of regulatory genes (44, 45). Erk1/2 activation has been shown to be required for cellular induction of p21 expression in response to mitogens (44, 46). Interestingly, we observed decreased p21 expression in BM KSL cells in *Kras*[ex3op/ex3op] mice in association with increased Erk1/2 phosphorylation. This could be explained by Erk1/2–mediated activation of c-Myc or c-Jun, which can repress transcription of p21 (44, 45, 47). p21 abrogates cell cycle progression via inhibition of Cdks, including Cdk2, Cdk4, and Cdk6 (34). Here, we demonstrated that administration of the Cdk4/6 inhibitor, palbociclib, repressed both in vitro hematopoietic colony formation and in vivo repopulating capacity of BM HSCs from *Kras*[ex3op/ex3op] mice, suggesting that Kras-mediated augmentation of HSC functional activity occurred via activation of Cdk4/6. The increased levels of p-Rb in BM KSL cells from *Kras*[ex3op/ex3op] mice further support this hypothesis. Consistent with our model, enforced expression of Cdk4 in human HSCs was previously shown to promote G_0 to G_1 transit and improved HSC repopulating capacity in NOD/SCID IL-2 receptor γ chain–deficient (NSG) mice (48). Cdk6 has also been shown to regulate the timing of murine HSC exit from quiescence while conferring a competitive repopulation advantage (49). Furthermore, Cdk4/6 inhibition was shown to protect HSCs from chemotherapy-induced exhaustion, in keeping with our observation that increased Kras signaling produced Cdk4/6 activation, yielding exhaustion of LT-HSCs in *Kras*[ex3op/ex3op] mice (50). Finally, our observation of HSC exhaustion in the *Kras*[ex3op/ex3op] mice in association with decreased p21 expression is consistent with prior studies showing that p21 deficiency increased HSC proliferation and number but decreased HSC serial repopulating capacity (51). Nonetheless, given the survival benefit demonstrated in *Kras*[ex3op/ex3op] mice following lethal dose TBI and in recipient mice following transplantation of BM cells from *Kras*[ex3op/ex3op] mice, short-term pharmacologic activation of Kras signaling may have therapeutic potential as a strategy to promote hematopoietic regeneration following myelosuppression. In order to clarify the potential therapeutic benefit of Kras activation, we will pursue additional studies characterizing the hematologic profiles of *Kras*[ex3op/ex3op] mice over time following sublethal irradiation and chemotherapy. In principle, a pharmacologic strategy to temporarily induce Kras signaling could harness the beneficial effects of Kras activation in HSCs while avoiding the exhaustion of HSCs that we have observed in mice with unrelieved Kras signal.

Since Kras activation can affect cells within the BM microenvironment (52), we also sought to determine whether the hematopoietic phenotype of *Kras*[ex3op/ex3op] mice was caused by hematopoietic cell–autonomous effects or via indirect effects through the BM niche. Interestingly, 8-week-old chimeric *nat;ex3op* mice displayed no expansion of BM HSCs, KSL progenitor cells, or B cells as was observed in *Kras*[ex3op/ex3op] mice.

This suggests that these effects of increased Kras protein on hematopoiesis occurred in a hematopoietic cell–autonomous manner, independent from any effects on the BM microenvironment. Of note, *nat;ex3op* mice displayed an increase in PB neutrophils compared with *nat;nat* control mice, suggesting the possibility that the *Kras ex3op* mutation in the BM niche may alter myeloid cell production or differentiation in vivo. This will be evaluated in depth in future studies.

Finally, our results suggest the intriguing possibility that natural variation in KRAS expression in the human population may contribute to observed variability in the regenerative potential of hematopoietic grafts from human BM or PB stem cell donors. Insufficient PB stem cell collection occurs in up to 15% of autologous donors and graft failure occurs in 5%–15% of adult transplant recipients of cord blood and from older BM donors (53–56). It would be of interest to determine if alterations in KRAS protein expression correlate with variations in human hematopoietic graft function. More broadly, this study provides principal demonstration of codon usage in a mammal having a biological consequence, which may speak to the importance of codon usage in mammalian biology.

Methods

Mice. All animal procedures were performed in accordance with animal use protocols approved by the UCLA Animal Care and Use Committee. Generation of the $Kras^{ex3op/ex3op}$ mouse has been previously reported (6). The $Kras^{ex3op/ex3op}$ mice were backcrossed 10 generations into C57BL/6 mice purchased from Jackson Laboratories (stock 000664). In some studies, $Kras^{ex3op/ex3op}$ mice were crossed into *β-actin-DsRed* mice (DsRed, stock 006051, Jackson Laboratories) to facilitate analysis of donor versus recipient hematopoietic cells. We measured complete blood counts using a Hemavet 950 instrument (Drew Scientific). For determination of cell-autonomous effects of $Kras^{ex3op}$ mutation on hematopoiesis, we transplanted 3×10^6 BM cells from wild-type littermate control ($Kras^{nat/nat}$) mice into irradiated (950 cGy) $Kras^{ex3op/ex3op}$ mice and $Kras^{nat/nat}$ mice (controls). At 8 weeks of age, we confirmed greater than 90% donor CD45.1$^+$ cell chimerism in the BM of transplanted mice (*nat;ex3op* mice). We subsequently measured the PB and BM hematopoietic profiles in *nat;ex3op* chimeric mice versus *nat;nat* control mice. We utilized 8- to 12-week-old, age- and sex-matched mice, with wild-type littermates as controls for all mice studies, except as otherwise noted.

Competitive repopulation assays. In order to perform primary competitive repopulation assays, $Kras^{ex3op/ex3op}$ mice and $Kras^{nat/nat}$ mice were backcrossed 10 or more generations into C57BL/6 background (CD45.2$^+$) and were utilized as donor mice. Syngeneic B6.SJL (CD45.1$^+$) mice (Jackson Laboratories, stock 002014) were used as recipients. An equal dose of donor BM cells (2×10^5) and competitor BM cells (2×10^5) was utilized for these experiments. Donor hematopoietic cell engraftment within myeloid cells, B cells, and T cells in transplanted mice was measured by flow cytometry, as previously described (24–27).

We also utilized $Kras^{ex3op/ex3op}$ mice and $Kras^{nat/nat}$ mice (C57BL/6 background) that were crossed into the *β-actin-DsRed* mice (C57BL/6 background) for competitive repopulation assays into lethally irradiated recipient 10-week-old female $Kras^{nat/nat}$ mice (DsRed-negative), following the approach described above. At 20 weeks after transplant, 1×10^6 BM cells were collected from primary recipient mice and injected via tail vein, along with 2×10^5 competitor (DsRed-negative) BM cells, into lethally irradiated secondary recipient $Kras^{nat/nat}$ mice (DsRed-negative). Measurement of donor hematopoietic cell engraftment within myeloid, B cell, and T cell lineages was performed as previously described (24–27).

Mouse cell isolation and culture. PB was collected from mice through submandibular puncture. To collect BM cells, long bones (femurs and tibia) were harvested from euthanized mice and flushed with IMDM containing 10% FBS. BM cells were filtered through a 40-μm strainer to obtain single-cell suspensions. Both PB and BM were subjected to RBC lysis using ACK RBC lysis buffer prior to FACS staining. Spleens were mechanically dissociated using a mortar and pestle and then subjected to RBC lysis. Single-cell suspensions of thymocytes were prepared by mechanical dissociation in buffer (10% FBS in PBS). We performed mouse BM lineage depletion using a mouse lineage cell depletion kit, per the manufacturer's protocol (Miltenyi Biotec). We cultured lineage-negative mouse HSCs and progenitor cells in IMDM with 10% FBS, 125 ng/ml mouse stem cell factor (SCF) (R&D Systems, 455-MC-010), 20 ng/ml mouse TPO (R&D Systems, 488-TO-005/CF), and 50 ng/ml mouse Fms-like tyrosine kinase 3 ligand (Ftl3L) (R&D Systems, 427-FL-005/CF). Where noted, palbociclib or BVD-523 was added to the media at 100 nM.

BrdU. BrdU (Sigma-Aldrich) was administered as a single dose of 150 mg per kg of body mass by intraperitoneal injection followed by 1 mg/ml BrdU in the drinking water. Analysis was performed at 24 hours. For long-term BrdU administration (5 and 25 days), BrdU water was given continuously and changed every 3 days.

Immune cell analysis and flow cytometry. Cells were analyzed by flow cytometry for myeloid (CD11b$^+$/Gr-1$^+$), B cell (B220$^+$), T cell (CD3$^+$), stem/progenitor cell (KSL), and HSCs as previously described (57, 58). Histograms and dot plots were created using FlowJo software (Tree Star). BrdU analysis was performed using the BrdU Flow Kit, following the manufacturer's instructions (BD, catalog number 559619). Briefly, cells were stained for extracellular antigens for 30 minutes on ice, fixed with Cytofix/Cytoperm (BD Biosciences, catalog number 554722) for 15 minutes, and then washed 3 times with PBS and incubated with intracellular antibody in 2% FBS in PBS for 30 minutes at room temperature. Analysis was performed on a FACSCanto II (BD).

For PB T cell staining, cells were labeled with V450-CD3 (BD Biosciences, 561389, 1:200), PE-CD4 (Biolegend, 100407, 1:200), BV605-CD8 (BD Biosciences, 563152, 1:200), APC/Cy7-CD44 (Biolegend, 103027, 1:200), FITC-CD62L (Biolegend, 104405, 1:200), and Alexa Fluor 647 CD45RA (BD Biosciences, 562763, 1:200). For B/NK cell staining, cells were labeled with V450-CD3 (BD Biosciences, 561389, 1:200), Alexa Fluor 647 NK1.1 (Biolegend, 108719, 1:200), PE-CD122 (Biolegend, 105905, 1:200), and FITC-CD19 (Biolegend, 152403 1:200). Corresponding isotypes were used to confirm antibody staining efficiency and compensation controls were used to set gates. Effector memory T cells (CD3$^+$CD4/8$^+$CD44$^+$CD62L$^-$), naive T cells (CD3$^+$CD4/8$^+$CD44$^-$CD62L$^+$), cytotoxic T cells (CD3$^+$CD8$^+$), B cells (CD3$^-$CD19$^+$), and NK cells (CD3$^-$CD19$^-$CD122$^+$NK1.1$^+$) were analyzed using FlowJo analysis software version 10. Numbers of each PB population were calculated by multiplying the percentages of each subset by the total WBCs in each sample.

The thymi of 8- to 10-week-old *Kras^nat/nat^* mice and *Kras^ex3op/ex3op^* mice were harvested and pressed through a 70-μm cell strainer (Falcon) with the plunger of a 3-ml syringe to obtain a cell suspension. Cells were kept in cold analysis medium (PBS 1×, 0.1% BSA, and 2 mM EDTA) throughout the entire experiment. Thymocytes were then counted using a hemacytometer (Hausser Scientific) and viability was determined by trypan blue exclusion (Sigma-Aldrich). For early T cell progenitor analysis, 25×10^6 to 50×10^6 thymocytes were incubated with purified anti-CD4 (clone RM4-5, BD Biosciences) and anti-CD8 antibodies (clone 53-6.7, BD Biosciences), in addition to a cocktail of antibodies (anti-CD11b, anti-CD16/32, anti-B220, and anti-TER119) from a Dynabeads Untouched T cells kit (Invitrogen). After magnetic isolation with Dynabeads, lineage negative (lin$^-$) thymocytes were then counted and stained with the following conjugated antibodies: anti-CD45 FITC (30-F11), anti-B220 PerCPCy5.5 (RA3-6B2), anti-CD11b PerCP-Cy5.5 (M1/70), anti-Gr1 PerCP-Cy5.5 (RB6-8C5), anti-TER119 PerCP-Cy5.5, anti-CD25 PE-Cy7 (PC61), anti-CD117 APC (2B8) (all BD Biosciences); anti-CD4 APC-Cy7 (GK1.5), anti-CD8 BV711 (53-6.7), anti-CD3 BV510 (17A2), and anti-CD44 BV786 (IM7) (all BioLegend). For total thymocyte analysis, 1×10^6 thymocytes were stained with the above-mentioned conjugated antibodies. For thymocyte maturation analysis, 1×10^6 total thymocytes were stained with the following conjugated antibodies: anti-CD45 PE (30-F11), anti-CD62L PerCP-Cy5.5 (MEL-14), anti-CD3 PE-Cy7 (17A2) (all BD Biosciences); anti-Qa2 FITC (695 H1-9-9), anti-CD8 APC-Cy7 (53-6.7), anti-CD69 BV510 (H1.2 F3), anti-CD4 BV605(GK1.5), and anti-CD24 BV711 (M1/69) (all BioLegend). Stained cells were then analyzed by flow cytometry (BD LSR Fortessa, BD Biosciences).

Phospho-flow cytometry. Following lineage depletion, BM cells were sorted for KSL cells. Cells were washed using IMDM with no FBS to serum starve for 30 minutes at 37°C. Subsequently, growth factor was added for 5 minutes prior to fixing by adding 10 volumes prewarmed Lyse/Fix buffer (BD Biosciences, 558049). Fixation was performed at 37°C for 10 minutes. Cells were washed in stain buffer (BD Biosciences, 554656), and then permeabilized with prechilled Perm Buffer III (BD Biosciences, 558050) on ice for 30 minutes. After washing with stain buffer 3 times, the cells were resuspended with the phospho-flow antibody at the recommended concentration overnight at 4°C prior to analysis. Antibodies were the following (all from BD Biosciences): Phosflow PE Mouse anti-Akt (pT308), 558275; Phosflow Alexa Fluor 647 Mouse anti-Akt (pS473), 560343; Phosflow Alexa Fluor 647 Mouse anti-S6 (pS244), 560465; Phosflow PE Mouse Anti-Stat5 (pY694), 612567; and PE Mouse Anti-ERK1/2 (pT202/pY204), 612566.

Immunohistochemical analysis. Freshly dissected femurs were decalcified using Surgipath Decalcifier II for 6 hours. Four-micron sections were created from formalin-fixed, paraffin-embedded blocks, using a rotary microtome, floated on a 49°C water bath, and mounted on a positively charged slide. All slides were baked overnight in a 65°C oven, stained with H&E, and then covered using resinous mounting medium. Paraffin-embedded sections were cut at 4-μm thickness and paraffin removed with xylene and rehydrated through graded ethanol. Images were acquired using a Zeiss Axio Imager M2.

Table 1. TaqMan primers

Gene	Assay ID
CCND1	Mm00432359_m1
CCND2	Mm00438070_m1
CDK8	Mm01223097_m1
p19 (CDKN2D)	Mm00486943_m1
p21 (CDKN1A)	Mm04205640_g1
p27 (CDKN1B)	Mm00438168_m1

Homing assay. $Kras^{nat/nat}$ mice (DsRed-negative) were irradiated with 900 cGy TBI. Using $Kras^{ex3op/ex3op};DsRed$ mice or $Kras^{nat/nat};DsRed$ mice as donors, we sorted BM KSL cells and injected 4×10^4 cells per recipient. We analyzed the BM at 18 hours after injection for DsRed$^+$ hematopoietic cells (59).

CFC assays. BM cells were plated in MethoCult GFM3434 (Stem Cell Technologies). Numbers of cells utilized and time of analysis are provided in the figure legends. Colonies were counted 14 days later, unless otherwise indicated by morphology. CFC assays (colony-forming unit–granulocyte monocyte [CFU-GM], burst-forming unit–erythroid [BFU-E], and CFU–granulocyte erythroid monocyte megakaryocyte [CFU-GEMM]) were performed as we have previously described (57).

LTC-IC assay. BM LTC-IC assay was performed as previously described (51), with minor modifications. Briefly, the unfractionated BM cells were plated on an irradiated (15 Gy) primary mouse stromal monolayer in 96-well plates containing 150 μl of M5300 medium (Stem Cell Technologies) supplemented with 10–6 M hydrocortisone. The media were changed with half-fresh medium weekly until week 5 when the cells were harvested with trypsin and plated for CFCs in M3434 media (Stem Cell Technologies). The plates were evaluated for the presence of CFCs 10 days thereafter.

Radiation studies. Ten-week-old male $Kras^{ex3op/ex3op}$ mice or $Kras^{nat/nat}$ mice were treated with 750 cGy TBI using a Cesium-137 irradiator. Mice were monitored daily through day +30 and euthanized as per our approved animal use protocol, if necessary. Complete blood counts were measured using a Hemavet 950 instrument (Drew Scientific). For the limiting-dose BM transplantation experiment, 8-week-old male C57BL/6 mice received 850 cGy TBI followed by tail vein injection of 1×10^5 BM cells from $Kras^{ex3op/ex3op}$ mice or $Kras^{nat/nat}$ mice. Palbociclib or vehicle was administered intraperitoneally on day +5 and +6 at 85 mg/kg, dissolved in sodium lactate. For competitive transplants or chimeric mice generation, 950 cGy TBI was used and BM cells were injected 24 hours later. Mice were monitored daily through day +30 and euthanized per our animal use protocol, if necessary.

PCR. We performed gene expression analysis via qRT-PCR on populations of BM KSL cells. RNA was isolated using the Qiagen RNeasy Micro Kit. RNA was reverse transcribed into cDNA using an iScript cDNA synthesis kit and random hexamers. Real-time PCR analysis was performed using TaqMan Gene Expression assays (Life Technologies) on an Applied Biosystems QuantStudio 6 PCR Machine (Thermo Fisher Scientific). The primers used for TaqMan-based PCR are shown in Table 1. Data were normalized to GAPDH and littermate controls using the double-delta CT method. For CDK1, CCNE1, and B-MYB, the SYBR Green method was used. cDNA (20 ng) was used for qPCR with the SYBR Select Master Mix (Life Technologies). The sequences of the primers used for SYBR Green–based PCR are shown in Table 2. Values were normalized using GAPDH.

Sanger sequencing. DNA sequencing of *Ras* genes was performed by Laragen, Inc., and performed on an ABI 3730XL sequencer using BigDye on a 3.1 sequencing reaction. Five $Kras^{nat/nat}$ mice and 5 $Kras^{ex3op/ex3op}$ mice were tested using primers flanking exons containing codons 12, 13, and 61 in *Kras*, *Nras*, and *Hras*.

Statistics. Values are represented as means ± SEM as noted in the figure legends. All comparisons were made using an unpaired 2-tailed Student's *t* test, unless otherwise indicated in the figure legends. A 2-sample equal variance with normal distribution was utilized and *P* values less than 0.05 were considered to be significant. GraphPad Prism 6.0 was used for all statistical analyses. All data were checked for normal distribution and similar variance between groups. Sample size for in vitro studies was chosen based on

Table 2. SYBR Green primer sequences

Gene	Forward Primer	Reverse Primer
GAPDH	TGGATTTGGACGCATTGGTC	TTTGCACTGGTACGTGTTGAT
CDK1	AGAAGGTACTTACGGTGTGGT	GAGAGATTTCCCGAATTGCAGT
B-MYB	TCTGGATGAGTTACACTACCAGG	GTGCGGTTAGGAAAGTGACTG
CCNE1	GTGGCTCCGACCTTTCAGTC	CACAGTCTTGTCAATCTTGGCA

observed effect sizes and standard errors from prior studies. For animal studies, a power test was used to determine the sample size needed to observe a 2-fold difference in means between groups with 0.8 power using a 2-tailed Student's t test. All animal studies were performed using sex- and age-matched animals, with wild-type littermates as controls. Animal studies were performed without blinding of the investigator and no animals were excluded from the analysis. Statistical details of each experiment are described in the figure legends, including the numbers of replicates and P values from the Student's t test.

Study approval. All animal studies were performed under UCLA animal care and use protocol 2014-021-13E (Principal Investigator, John Chute), approved by the UCLA Animal Care and Use Committee.

Author contributions

JPC designed and directed the study. JPS, HAH, ET, JK, ML, YZ, MR, CMT, and SCDB performed experiments reported in this study. LZ performed mouse breeding and maintenance. DSR analyzed tissue sections to evaluate for malignancy and provided guidance on experimental design. CMC provided the transgenic mice and guidance on experimental design. JPS, CMC, and JPC wrote the manuscript with input from all the authors.

Acknowledgments

Address correspondence to: John P. Chute, University of California, Los Angeles, Eli and Edythe Broad Center for Stem Cell Research, Jonsson Comprehensive Cancer Center, Orthopedic Hospital Research Center Building, Room 547, 617 Charles E. Young Drive South, Los Angeles, California 90095, USA. Phone: 310.206.4929; Email: jchute@mednet.ucla.edu.

1. Pershing NL, Lampson BL, Belsky JA, Kaltenbrun E, MacAlpine DM, Counter CM. Rare codons capacitate Kras-driven de novo tumorigenesis. *J Clin Invest*. 2015;125(1):222–233.
2. Ali M, et al. Codon bias imposes a targetable limitation on KRAS-driven therapeutic resistance. *Nat Commun*. 2017;8:15617.
3. Pylayeva-Gupta Y, Grabocka E, Bar-Sagi D. RAS oncogenes: weaving a tumorigenic web. *Nat Rev Cancer*. 2011;11(11):761–774.
4. Stephen AG, Esposito D, Bagni RK, McCormick F. Dragging ras back in the ring. *Cancer Cell*. 2014;25(3):272–281.
5. Ahearn IM, Haigis K, Bar-Sagi D, Philips MR. Regulating the regulator: post-translational modification of RAS. *Nat Rev Mol Cell Biol*. 2011;13(1):39–51.
6. Lampson BL, et al. Rare codons regulate KRas oncogenesis. *Curr Biol*. 2013;23(1):70–75.
7. Nakamura Y, Gojobori T, Ikemura T. Codon usage tabulated from international DNA sequence databases: status for the year 2000. *Nucleic Acids Res*. 2000;28(1):292.
8. MacKenzie KL, Dolnikov A, Millington M, Shounan Y, Symonds G. Mutant N-ras induces myeloproliferative disorders and apoptosis in bone marrow repopulated mice. *Blood*. 1999;93(6):2043–2056.
9. Braun BS, et al. Somatic activation of oncogenic Kras in hematopoietic cells initiates a rapidly fatal myeloproliferative disorder. *Proc Natl Acad Sci USA*. 2004;101(2):597–602.
10. Van Meter ME, et al. K-RasG12D expression induces hyperproliferation and aberrant signaling in primary hematopoietic stem/progenitor cells. *Blood*. 2007;109(9):3945–3952.
11. Sabnis AJ, et al. Oncogenic Kras initiates leukemia in hematopoietic stem cells. *PLoS Biol*. 2009;7(3):e59.
12. Li Q, et al. Hematopoiesis and leukemogenesis in mice expressing oncogenic NrasG12D from the endogenous locus. *Blood*. 2011;117(6):2022–2032.
13. Li Q, et al. Oncogenic Nras has bimodal effects on stem cells that sustainably increase competitiveness. *Nature*. 2013;504(7478):143–147.
14. Xu J, et al. Dominant role of oncogene dosage and absence of tumor suppressor activity in Nras-driven hematopoietic transformation. *Cancer Discov*. 2013;3(9):993–1001.
15. Lyubynska N, et al. A MEK inhibitor abrogates myeloproliferative disease in Kras mutant mice. *Sci Transl Med*. 2011;3(76):76ra27.
16. Hawley RG, Fong AZ, Ngan BY, Hawley TS. Hematopoietic transforming potential of activated ras in chimeric mice. *Oncogene*. 1995;11(6):1113–1123.
17. Dorrell C, Takenaka K, Minden MD, Hawley RG, Dick JE. Hematopoietic cell fate and the initiation of leukemic properties in primitive primary human cells are influenced by Ras activity and farnesyltransferase inhibition. *Mol Cell Biol*. 2004;24(16):6993–7002.
18. Tarnawsky SP, Kobayashi M, Chan RJ, Yoder MC. Mice expressing KrasG12D in hematopoietic multipotent progenitor cells

develop neonatal myeloid leukemia. *J Clin Invest*. 2017;127(10):3652–3656.

19. Akutagawa J, et al. Targeting the PI3K/Akt pathway in murine MDS/MPN driven by hyperactive Ras. *Leukemia*. 2016;30(6):1335–1343.

20. Damnernsawad A, et al. Kras is required for adult hematopoiesis. *Stem Cells*. 2016;34(7):1859–1871.

21. Himburg HA, et al. Pleiotrophin regulates the expansion and regeneration of hematopoietic stem cells. *Nat Med*. 2010;16(4):475–482.

22. Himburg HA, et al. Pleiotrophin mediates hematopoietic regeneration via activation of RAS. *J Clin Invest*. 2014;124(11):4753–4758.

23. Signer RA, Magee JA, Salic A, Morrison SJ. Haematopoietic stem cells require a highly regulated protein synthesis rate. *Nature*. 2014;509(7498):49–54.

24. Silberstein L, et al. Proximity-based differential single-cell analysis of the niche to identify stem/progenitor cell regulators. *Cell Stem Cell*. 2016;19(4):530–543.

25. Mercier FE, Sykes DB, Scadden DT. Single targeted exon mutation creates a true congenic mouse for competitive hematopoietic stem cell transplantation: The C57BL/6-CD45.1(STEM) mouse. *Stem Cell Reports*. 2016;6(6):985–992.

26. Chen JY, et al. Hoxb5 marks long-term haematopoietic stem cells and reveals a homogenous perivascular niche. *Nature*. 2016;530(7589):223–227.

27. Li Q, et al. Oncogenic Nras has bimodal effects on stem cells that sustainably increase competitiveness. *Nature*. 2013;504(7478):143–147.

28. Fleming HE, et al. Wnt signaling in the niche enforces hematopoietic stem cell quiescence and is necessary to preserve self-renewal in vivo. *Cell Stem Cell*. 2008;2(3):274–283.

29. Quarmyne M, et al. Protein tyrosine phosphatase-σ regulates hematopoietic stem cell-repopulating capacity. *J Clin Invest*. 2015;125(1):177–182.

30. Bourne HR, Sanders DA, McCormick F. The GTPase superfamily: a conserved switch for diverse cell functions. *Nature*. 1990;348(6297):125–132.

31. Bourne HR, Sanders DA, McCormick F. The GTPase superfamily: conserved structure and molecular mechanism. *Nature*. 1991;349(6305):117–127.

32. Boguski MS, McCormick F. Proteins regulating Ras and its relatives. *Nature*. 1993;366(6456):643–654.

33. Tan PB, Kim SK. Signaling specificity: the RTK/RAS/MAP kinase pathway in metazoans. *Trends Genet*. 1999;15(4):145–149.

34. Harper JW, et al. Inhibition of cyclin-dependent kinases by p21. *Mol Biol Cell*. 1995;6(4):387–400.

35. Xiong Y, Hannon GJ, Zhang H, Casso D, Kobayashi R, Beach D. p21 is a universal inhibitor of cyclin kinases. *Nature*. 1993;366(6456):701–704.

36. Chang F, Steelman LS, McCubrey JA. Raf-induced cell cycle progression in human TF-1 hematopoietic cells. *Cell Cycle*. 2002;1(3):220–226.

37. Rubin SM. Deciphering the retinoblastoma protein phosphorylation code. *Trends Biochem Sci*. 2013;38(1):12–19.

38. Lundberg AS, Weinberg RA. Functional inactivation of the retinoblastoma protein requires sequential modification by at least two distinct cyclin-cdk complexes. *Mol Cell Biol*. 1998;18(2):753–761.

39. Lam EW, Watson RJ. An E2F-binding site mediates cell-cycle regulated repression of mouse B-myb transcription. *EMBO J*. 1993;12(7):2705–2713.

40. DeGregori J, Kowalik T, Nevins JR. Cellular targets for activation by the E2F1 transcription factor include DNA synthesis- and G1/S-regulatory genes. *Mol Cell Biol*. 1995;15(8):4215–4224.

41. Furukawa Y, Terui Y, Sakoe K, Ohta M, Saito M. The role of cellular transcription factor E2F in the regulation of cdc2 mRNA expression and cell cycle control of human hematopoietic cells. *J Biol Chem*. 1994;269(42):26249–26258.

42. Castellano E, Santos E. Functional specificity of ras isoforms: so similar but so different. *Genes Cancer*. 2011;2(3):216–231.

43. Parikh C, Subrahmanyam R, Ren R. Oncogenic NRAS, KRAS, and HRAS exhibit different leukemogenic potentials in mice. *Cancer Res*. 2007;67(15):7139–7146.

44. Meloche S, Pouysségur J. The ERK1/2 mitogen-activated protein kinase pathway as a master regulator of the G1- to S-phase transition. *Oncogene*. 2007;26(22):3227–3239.

45. Shaulian E, Karin M. AP-1 in cell proliferation and survival. *Oncogene*. 2001;20(19):2390–2400.

46. Liu Y, Martindale JL, Gorospe M, Holbrook NJ. Regulation of p21WAF1/CIP1 expression through mitogen-activated protein kinase signaling pathway. *Cancer Res*. 1996;56(1):31–35.

47. Shaulian E, Schreiber M, Piu F, Beeche M, Wagner EF, Karin M. The mammalian UV response: c-Jun induction is required for exit from p53-imposed growth arrest. *Cell*. 2000;103(6):897–907.

48. Mende N, et al. CCND1-CDK4-mediated cell cycle progression provides a competitive advantage for human hematopoietic stem cells in vivo. *J Exp Med*. 2015;212(8):1171–1183.

49. Laurenti E, et al. CDK6 levels regulate quiescence exit in human hematopoietic stem cells. *Cell Stem Cell*. 2015;16(3):302–313.

50. He S, et al. Transient CDK4/6 inhibition protects hematopoietic stem cells from chemotherapy-induced exhaustion. *Sci Transl Med*. 2017;9(387):eaal3986.

51. Cheng T, et al. Hematopoietic stem cell quiescence maintained by p21cip1/waf1. *Science*. 2000;287(5459):1804–1808.

52. Ichise T, Yoshida N, Ichise H. H-, N- and Kras cooperatively regulate lymphatic vessel growth by modulating VEGFR3 expression in lymphatic endothelial cells in mice. *Development*. 2010;137(6):1003–1013.

53. To LB, Levesque JP, Herbert KE. How I treat patients who mobilize hematopoietic stem cells poorly. *Blood*. 2011;118(17):4530–4540.

54. Arai Y, et al. Allogeneic unrelated bone marrow transplantation from older donors results in worse prognosis in recipients with aplastic anemia. *Haematologica*. 2016;101(5):644–652.

55. Cutler C, et al. Donor-specific anti-HLA antibodies predict outcome in double umbilical cord blood transplantation. *Blood*. 2011;118(25):6691–6697.

56. Kanda J, et al. Adult dual umbilical cord blood transplantation using myeloablative total body irradiation (1350 cGy) and fludarabine conditioning. *Biol Blood Marrow Transplant*. 2011;17(6):867–874.

57. Yan X, et al. Deletion of the imprinted gene Grb10 promotes hematopoietic stem cell self-renewal and regeneration. *Cell Rep*. 2016;17(6):1584–1594.

58. Himburg HA, et al. Dickkopf-1 promotes hematopoietic regeneration via direct and niche-mediated mechanisms. *Nat Med*. 2017;23(1):91–99.

59. Christopherson KW, Hangoc G, Mantel CR, Broxmeyer HE. Modulation of hematopoietic stem cell homing and engraftment by CD26. *Science*. 2004;305(5686):1000–1003.